Paspalum notatum Grass-waste-based Adsorbent for Rhodamine B Removal from Polluted Water

A. Zahir,[a] Z. Aslam,[b,*] U. Aslam,[b] A. Abdullah,[b] R. Ali,[b] and M. M. Bello[c]

[a]National Textile Research Centre, National Textile University, Faisalabad, 37610, Pakistan

[b]Department of Chemical Engineering, University of Engineering and Technology, Lahore, 54890, Pakistan

[c]Department of Chemical Engineering, Faculty of Engineering, University of Malaya, 50603 Kuala Lumpur, Malaysia

https://doi.org/10.15255/CABEQ.2020.1830

Original scientific paper
Received: May 26, 2020
Accepted: July 24, 2020

The potential of *Paspalum notatum* grass waste to adsorb Rhodamine B dye from aqueous phase is reported in this research. The grass waste was activated and characterized through various techniques to analyze the chemical (FTIR), morphological (SEM-EDX), and thermal (TGA) changes incorporated through the activation process. The pollutant removal efficiency of the raw and modified adsorbents was studied by varying different process parameters in a batch process. The maximum capacity of adsorption which was observed for grass waste and activated grass waste was 54 mg g^{-1} and 72.4 mg g^{-1} respectively. Among the various kinetic models, the pseudo-second order model gives the best regression results. However, the intraparticle diffusion-adsorption model showed that the diffusion within pores controlled the adsorption rate. Thermodynamic analysis of this process revealed that Rhodamine B adsorption was endothermic and spontaneous in nature. The results of this study show that grass waste has the potential to be used as an adsorbent for the treatment of colored water.

Keywords:
biosorption, grass waste, *Paspalum notatum*, Rhodamine B, wastewater

Introduction

Organic dyes are used in various industries such as polymer, printing, paper and pulp, textile, and cosmetics to increase the aesthetics of their final products. Most of these dyes are hazardous due to their acute and chronic health effects, some being classified as carcinogenic. Therefore, the discharge of dyes into an aqueous environment poses a serious threat to human as well as aquatic life[1]. Among the toxic organic dyes, Rhodamine B is widely utilized in textile dying and in laboratories as a biological stain. Rhodamine B has been banned in food processing applications because of its carcinogenic nature. Therefore, it is imperative to either remove or minimize its concentration in wastewater to a safer limit before discharging into aquatic streams[2,3]. Various treatment methods, such as Fenton oxidation, photocatalytic oxidation, adsorption, coagulation, and membrane separation have been used to treat dye-containing wastewater[4–7]. Adsorption is one of the most economical, feasible, and cost-effective technologies. Activated carbon is used extensively as a conventional adsorbent due to its enhanced surface reactivity, high surface area, and high adsorption capacity. However, commercial activated carbon is quite expensive. Moreover, the reusability of activated carbon is still a challenge due to the loss of 10–15 % activated carbon during the regeneration process, which increases the overall treatment cost[8]. Therefore, adsorption of dyes using cheaper materials, such as agricultural wastes, has gained great attention. It has been estimated that about 1000/million tons of agricultural waste are being produced annually worldwide, but due to lack of resources, this waste cannot be utilized to its full potential. However, agricultural waste has received wide interest nowadays in the field of wastewater treatment due to its abundant availability, low cost, and ease of modification[9–11].

Various agro-based adsorbents have been researched for the treatment of dye-bearing effluents. Some of the agricultural wastes used as adsorbents include date palm fibers[12], banana fibers[13], straw[14], sugar cane bagasse[15], *Artocarpus odoratissimus* stem axis[16], water lettuce[17], *Artocarpus altilis* (breadfruit)[18], durian seed[19], orange peel[20], wheat husk[21]. Ramaraju studied the performance of nitric acid-modified and peroxide-modified rice husks for malachite green removal from aqueous solution. They reported that the adsorption capacity of perox-

*Corresponding author: hmzaheer@uet.edu.pk

ide-modified rice husk (26.6 mg g^{-1}) was superior to that of nitric acid-modified rice husk[11]. Hameed studied the potential of grass for the removal of methylene blue and reported an excellent adsorption capacity of 458 mg g^{-1} [9]. Kumar and Porkodi investigated the adsorption of methylene blue in *Paspalum notatum* by studying mass transfer and adsorption kinetics. They reported that the adsorption potential of *Paspalum notatum* was observed to be 31 mg g^{-1} [22]. The adsorption capacity of grass can be enhanced by modifying its physical/chemical structure. Chen *et al.* stated that the acid treatment of lawn grass increased its removal efficiency threefold for methylene blue adsorption[23]. The enhancement in the adsorption capacity was attributed to the increased surface functional groups induced by the chemical treatment. Cellulose, hemicellulose, lignin, and limonene are the main constituents of any grass, which provide additional functional groups, i.e., carboxyl, hydroxyl, and phenol. These functional groups can also be modified by different surface treatments of the grass to increase its affinity towards pollutants[24]. Kumar *et al.* removed lignin from the core of *Vetiveria zizanioides* grass and reported higher adsorption of chromium due to an increase in the surface area[25]. Different types of modified grass were already tested for the removal of many pollutants. However, there is a lack of studies for the use of acid-treated *Paspalum notatum* grass for Rhodamine B removal.

The aim of the current research work was to compare the adsorption capacity of *Paspalum notatum*, chlorophyll, and limonene-removed *Paspalum notatum* for Rhodamine B removal. The experiments were conducted through the batch adsorption process, and the effects of different process parameters were investigated. The synthesized adsorbent was analyzed for spectroscopic and surface properties by Fourier Transform Infrared Spectroscopy (FTIR) and Scanning Electron Microscopy (SEM), respectively. The experimental results were also analyzed thermodynamically and kinetically to study the spontaneity and adsorption mechanism.

Experimental

Materials

Paspalum notatum grass waste (GW) was collected from the stadium grounds of the University of Engineering and Technology, Lahore, Pakistan. Sodium hydroxide (≥97.0 %), isopropanol (99.5 %), and hydrochloric acid (37 %) were purchased from Sigma Aldrich. Rhodamine B ($C_{28}H_{31}ClN_2O_3$, Assay ≥ 98 %, mol. wt. 479.01) was purchased from ACROS Organics. Analytical grade reagents were used without prior purification.

Preparation and characterization

Preparation of adsorbent

The GW was firstly cleaned with demineralized water to wash the mud and dirt from its surface. The washed sample was dried at 60 °C in an oven for 24 h. The low temperature was selected to avoid thermal deactivation of the surface of the grass. The dried GW was ground and sieved to obtain a uniform particle size. Fifty grams of ground GW powder was soaked in a beaker containing 500 mL of 1 M isopropanol solution. The GW powder was left to soak for 24 hours to remove organic constituents such as chlorophyll and limonene. After filtration, the mixture residue was cleaned with double demineralized water until a colorless filtrate was observed. The residue was then dried at 60 °C in an oven for 24 h. The chlorophyll-removed GW powder was then subjected to acid activation. Twenty grams of chlorophyll-removed GW powder was boiled in 500 mL of 0.75 M HCl solution under total reflux conditions for 4 hours. The solid was then filtered and the residue rinsed several times with demineralized water to remove the acid contents. The solid residue was then dried at 80 °C in an oven for 24 h. The dried acid-treated GW was sealed in an airtight jar for further use. The acid-activated GW is further herein abbreviated as "AGW".

Material characterization

The IR spectra of raw and activated GW were recorded on the FTIR spectrometer (Perkin Elmer, Spectrum two, USA) using ZnSe-ATR (Attenuated total reflectance) module. A half-gram of the sample was kept in a desiccator before the analysis in order to remove the adsorbent moisture. The thermal stability of the adsorbent was analyzed by a thermogravimetric analyzer (TA instrument, SDT-Q600, UK Ltd.). The analysis was performed in a nitrogen environment over the temperature range 30–900 °C at 10 °C min^{-1}. The surface morphological property was observed on Field Emission Scanning Electron Microscope **(**MIRA3, TESCAN, Cambridgeshire, UK**)** at 20 kV accelerating voltage. BET (Brunauer–Emmett–Teller) surface area of raw and modified grass was determined using the Micromeritics ASAP2020 analyzer.

Adsorption experiments

The adsorption of Rhodamine B dye was tested through the batch adsorption process. Accurately weighted Rhodamine B was dissolved in 1 L demineralized water to prepare a 100 ppm stock solution of dye. The required volume of stock solution was further diluted to obtain 100 mL of working solution of desired Rhodamine B concentration in

an Erlenmeyer flask. The working solution pH was maintained by 0.1 M solutions of NaOH and HCl. Initially, 0.3 g adsorbent dose was taken into solution and put on a multi-point orbital shaker at 150 rpm for 6 hours. The solution was filtered, and the filtrate analyzed using UV-Vis-NIR double beam spectrophotometer (Perkin Elmer Lambda 950, UK) at λ_{max} = 550 nm to determine the removal efficiency. No sorption was observed either on the filter paper or on the glassware. The effects of adsorbent dosage (0.05 – 4 g), time (1 – 390 min), initial concentration (10 to 500 ppm), pH (2–10), and temperature (20 to 50 °C) on the adsorption process were studied. The quantity of the adsorbed dye was calculated using Equations 1 and 2.

$$\%\ \text{removal} = \frac{\gamma_i - \gamma_{fe}}{\gamma_i} \cdot 100 \tag{1}$$

$$q_e = \frac{V\left(\gamma_i - \gamma_{fe}\right)}{w} \tag{2}$$

where, q_e (mg g^{-1}) is the equilibrium uptake capacity, V is the solution volume (L), γ_i (mg L^{-1}) is the initial Rhodamine B concentration in solution, γ_{fe} (mg L^{-1}) is the final Rhodamine B concentration in solution at equilibrium, and w is the adsorbent weight (g).

Adsorption kinetics

Various proposed kinetic models provide useful data of adsorption mechanism in order to enhance the adsorption capability and scale-up the feasibility of the adsorption process. Among these models, pseudo-first order describes the rate of adsorption uptake as a linear function of the gradient of adsorption. The linear formation of pseudo-first order kinetic model can be presented by Eq. 3.

$$\log\left(q_e - q_t\right) = \log q_e - \frac{K_1 t}{2.303} \tag{3}$$

where, K_1 (min^{-1}) is pseudo-first order constant, q_e (mg g^{-1}) and q_t (mg g^{-1}) are the equilibrium and instantaneous adsorption uptake of Rhodamine B over sorbent surface, respectively. The intercept and the slope of "t" vs log ($q_e - q_t$) plot may determine the parameter of the pseudo-first order model. The pseudo-second order model is given as Eq. 4.

$$\frac{t}{q_t} = \frac{1}{k_2 q_e^2} + \frac{t}{q_e} \tag{4}$$

where, k_2 (g mg g^{-1}) is pseudo-second order kinetic rate constant. Intercept and slope of the plot of t vs $\frac{t}{q_e}$ may be used to estimate the parameters of pseudo-second order model, i.e., k_2 and q_e.

The Elovich kinetic model, in its empirical form, has been used extensively to explain the chemisorption and surface heterogeneity of the adsorbent[26]. The linear formation of the Elovich kinetic model is given as Eq. 5.

$$q_t = \frac{1}{\beta}\ln\left(\alpha\beta\right) + \frac{1}{\beta}\ln\left(t\right) \tag{5}$$

where, α is a constant associated with the rate of chemisorption, and β is related to the surface coverage of sorbent by the Rhodamine B. The plot of q_t vs ln(t) is usually used to determine the α and β parameters.

The intraparticle diffusion model was employed in order to investigate the mechanism of diffusion of adsorbate, i.e., film diffusion, surface diffusion, or pore diffusion. The mathematical relation of the intraparticle diffusion model proposed by Weber and Morris is given by Equation 6.

$$q_t = k_i\sqrt{t} + \alpha \tag{6}$$

where, k_i (mg g^{-1} min$^{-\frac{1}{2}}$)is a constant of this model, and α (mg g^{-1}) corresponds to the boundary layer thickness at the interface of solid-liquid. The boundary layer influence will increase at its higher value, while intraparticle diffusion will be taken as only rate-limiting step if "α" is zero.

To investigate the pore diffusion step in the adsorption of Rhodamine B by GW and AGW, the Bangham model was used. If intraparticle diffusion is the only rate-limiting step in the adsorption, then the Bangham model plot should be a straight line (linear). However, non-linearity along with intercept depicted both the film diffusion as well as pore diffusion as the rate-limiting steps in the adsorption process. The linear form of the Bangham model can be written as Eq. 7 [27].

$$\log.\log\left(\frac{\gamma_i}{\gamma_i - q_t w}\right) = \log\left(\frac{K_b}{2.303V}\right) + \beta\log\left(t\right) \tag{7}$$

where, γ_i (mg L^{-1}) is the initial concentration of Rhodamine B, w (g) is the weight per liter of the adsorbent, and K_b and β are the constants of the Bangham model, and that can be estimated by the intercept and slope, respectively.

Adsorption isotherms

The distribution of pollutant over the solid surface can be explained by various models of equilibrium adsorption isotherm, i.e., Langmuir, Freundlich, and Redlich-Peterson (RP) isotherm models[28,29]. Moreover, isotherm analysis can also be used to determine the maximum uptake potential of an adsorbent for the scale-up of the adsorption process. Two- and three-parameter models were employed in this study.

Langmuir isotherm (two-parameter model) assumes constant enthalpy and activation energy of each active site on the sorbent surface. Furthermore, the Langmuir isotherm model assumes that no hindrance is caused by the nearby active site, and thus, reveals monolayer adsorption of dye molecules on the adsorbent homogeneous surface[30]. The mathematical expression of this model is represented as Equation 8.

$$q_e = q_m K_L \frac{\gamma_e}{1 + K_L \gamma_e} \tag{8}$$

where, q_m (mg L^{-1}) is the maximum uptake adsorption capacity, and K_L (L mg^{-1}) is the constant of the Langmuir model associated with the free energy of the adsorption process.

Freundlich isotherm (two-parameter model) presupposes that the adsorption activation energy varies for each active site. Therefore, it depicts the multilayer adsorption of pollutant on the adsorbent surface due to heterogeneity[31]. The non-linear expression for the Freundlich isotherm model can be expressed as Eq. 9.

$$q_e = K_F \gamma_e^{1/n} \tag{9}$$

where, K_F (mg g^{-1}) is a constant associated with relative uptake capacity of adsorbent, and n gives the heterogeneity of the surface.

Redlich-Peterson is a three-parameter isotherm model that includes the characteristics of both Langmuir and Freundlich models, and is therefore used as a compromise between the two isotherm models. The ratio of K_R/α_R depicts the maximum adsorption capacity of the adsorbent. The non-linear mathematical statement for Redlich-Peterson isotherm is given in Eq. 10[32].

$$q_e = \frac{K_R \gamma_e}{1 + \alpha_R \gamma_e^{\beta}} \tag{10}$$

where, K_R and β are the constants of the Redlich-Peterson isotherm model. This isotherm model is transformed to the Langmuir model when the parameter β is reduced to unity, and deduced to the Freundlich isotherm model as the value of $\alpha_R \gamma_e^{\beta}$ goes higher than 1. The coefficient of correlation (R^2) determines the validity of the model with experimental adsorption data. The predicted values from the modeled equation were also compared with experimental values in terms of an error function. Three error functions (Equations 11 – 13) were used for this purpose[33].

$$\text{Sum of the absolute error} = \text{SABE} = \sum_{i=1}^{N} \left[q_{e,exp} - q_{e,cal} \right] \tag{11}$$

$$\text{Hybrid fractional error function} = \text{HYBRID} = \frac{100}{n-p} \sum_{i=1}^{N} \frac{\left[q_{e,exp} - q_{e,cal} \right]^2}{q_{e,exp}} \tag{12}$$

$$\text{Non-Linear Chi-square} = \chi^2 = \sum_{i=1}^{N} \frac{\left(q_{e,cal} - q_{e,exp} \right)^2}{q_{e,exp}} \tag{13}$$

where n is the number of data points, and p is the total number of parameters in the model under consideration.

Adsorption thermodynamics

Thermodynamic variables, i.e., Gibb's free energy, enthalpy, and entropy are imperative to assess the practicality and nature of the adsorption process. Eqs. 14 – 16 were used for the thermodynamic analysis of the adsorption process.

$$K = \frac{\gamma_A}{\gamma_S} \tag{14}$$

$$\Delta G = -RT \ln K \tag{15}$$

$$\ln K = \frac{\Delta S}{R} - \frac{\Delta H}{RT} \tag{16}$$

where, K is the dimensionless distribution coefficient for the adsorption process, γ_A is Rhodamine B concentration on the adsorbent surface, γ_S is filtrate concentration of Rhodamine B, T (K) is the absolute temperature, R is the universal gas constant, ΔG (kJ mol^{-1}) is the change in Gibb's energy, ΔS (kJ mol^{-1}) is the change in entropy, and ΔH (kJ mol^{-1}) is the enthalpy change during the adsorption process.

Results and discussion

FTIR study

GW and AGW infrared spectra are shown in Fig. 1. For GW, the two acuminated peaks at wavenumbers 3848 cm^{-1} and 3744 cm^{-1} belong to the isolated OH functional groups in the organo-silicon compounds of the grass biomass. A broad and sharp peak centered at 3362 cm^{-1} may be attributed to stretching vibrations of hydrogen-bonded hydroxyl functional group that is associated with either polysaccharides or silanol compounds. The two consecutive peaks at 2922 cm^{-1} and 2848 cm^{-1} are ascribed to symmetric and asymmetric extension and contraction of C–H in the saturated hydrocarbons/carbohydrates containing methyl and methylene functional groups. The sturdy peak at 2358 cm^{-1} shows the occupancy of adsorbed CO_2 from the environment[34]. The transmittance peaks at 1689 and 1649 cm^{-1} may be linked to the stretching vibrations of C=C present in unconjugated cis-alkenes. The peak at 1741 cm^{-1} corresponds to the stretching vibrations of –C=O in the GW. Moreover, the small peak at 1531 cm^{-1} is probably because of the interaction of C–N stretching and N–H bending. The transmit-

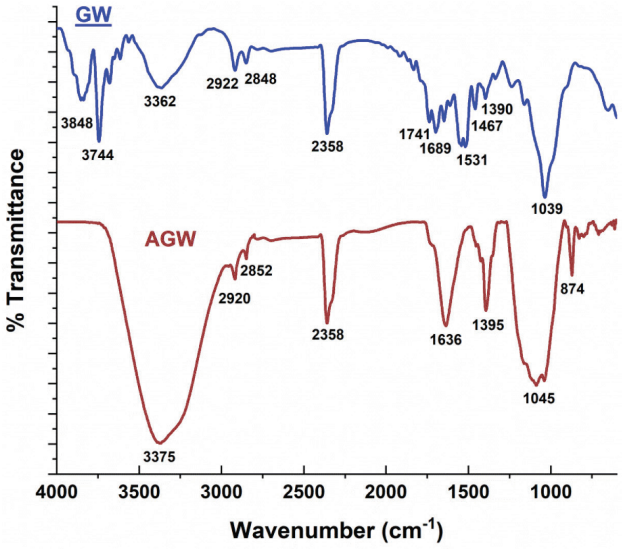

Fig. 1 – *Fourier transform infrared (FTIR) spectrum of GW and AGW*

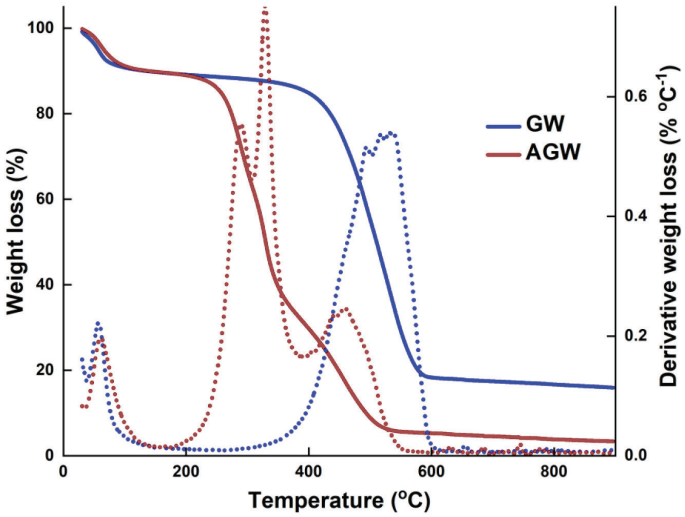

Fig. 2 – *Thermogravimetric analysis of GW and AGW*

tance peaks at 1390 cm^{-1} emanate from the in-phase and out-of-phase bending vibrations of two $–CH_3$ functional groups attached to a common carbon in the grass. The broad peak that has a minimum at 1039 cm^{-1} is associated with C–O stretching vibrations, asymmetric stretching mode of Si–O–Si, strong stretching vibrations of Si–O and C–H out-of-plane bending. The activation of GW imparted significant changes in the grass structure, as shown in Fig. 1 for AGW. The absence of peaks at higher wavenumbers (i.e., 3848 cm^{-1} and 3744 cm^{-1}) may have been due to the dissolution of limonene as a result of the alcoholic pretreatment and acid leaching of the grass[35]. Furthermore, the peak at 1531 cm^{-1} vanished, which reflects the removal of the amide II present in chlorophyll. The exclusion of these peaks in AGW confirms the successful removal of chlorophyll and limonene from the raw grass[23,36]. The activation processes increase the aromaticity in AGW by removing silica and other compounds, resulting in the presence of a sharp transmittance peak at 874 cm^{-1}.

Thermogravimetric analysis

The thermograms of both GW and AGW are summarized in Fig. 2. The mass loss pattern of GW exhibits two major phases, while the degradation of AGW displays four distinct phases in the examined temperature range. The first phase (caped between 33 °C to 148 °C) is the same for both GW and AGW, and approximately 10 % of total mass loss occurred in this range. This mass loss may be associated with the release of the water molecules and light volatiles retained on the adsorbent surface. The thermal decomposition of GW in the range of 290 °C – 600 °C gives a major loss in weight as represented by a broader peak in the derivative weight loss curve. This corresponds to the volatilization of the oxygenated compounds, i.e., cellulose, hemicellulose, and lignin in the GW[37,38]. For AGW, the thermal degradation starts a little earlier at around 167 °C and ends at 575 °C, after which the mass loss becomes constant. This decrease in the initial degradation temperature in AGW is due to the removal of chlorophyll from the grass, which binds the lignin chains through hydrogen bonding. The removal of chlorophyll induced thermal instability in the grass. Moreover, the acid activation reduces the polysaccharides and carbohydrates in GW, which decreases its resistance towards thermal degradation[39,40]. The broad tailing peak in AGW represents the char oxidation, which was not observable in GW due to the overlapping of decomposition temperatures of the oxygenated compounds. Raw GW may have a more complex structure because of overlapping saccharide compounds as compared to AGW. In addition, the activation process induced a structural and compositional change, which produced distinct sharp peaks in AGW, as may be observed in Fig. 2. Moreover, the percentage of the residual weight of GW was higher (i.e., 16 %) as compared to AGW, due to the higher content of impurities in GW.

SEM/EDX and porosity analysis

The surface morphologies of GW and AGW are presented in Fig. 3. Prominent textural changes are observable on the grass surface before and after activation. The surface of GW appears to be rough, uneven, defibrillated, and replete with surface impurities (Fig. 3a). Whereas, the activation process abraded the surface of the grass and created non-uniform/irregular cavities at the surface, as may be seen in Fig. 3b. Apparently, there is no major change

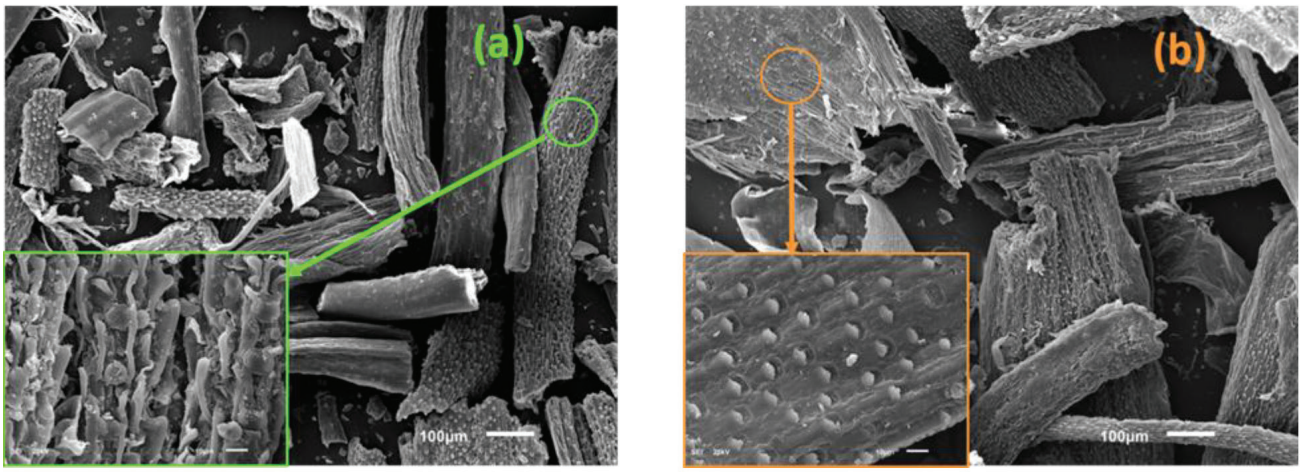

Fig. 3 – *SEM micrographs of (a) GW, and (b) AGW*

in the framework of the grass, which indicates that the grass has good mechanical properties. The porosity analysis revealed that the BET surface area of GW was 0.0068 m^2 g^{-1}, and after acid activation, the surface area of AGW was 0.35 m^2 g^{-1}. An increase in surface area is in agreement with SEM images in Fig. 3. The variations in the composition of elements were determined by spot analysis using EDX spectroscopy, and results are reported in Table 1. Ca and Fe were completely removed from AGW, because the acid activation leached all inorganic mineral impurities. However, a relative increase in silica weight percentage was observed, which showed its inherent characteristic of being insoluble in acid.

Analysis of adsorption process parameters

The viability of the adsorption process strongly depends on the amount of adsorbent required to abate the pollutant from the aqueous phase. The adsorbent dosage effect on the uptake of Rhodamine B is presented in Table 2. The higher percentage removal of pollutant may be observed by increasing dosage of the adsorbent for both AGW and GW. This is probably because of the availability of a greater number of active sites for Rhodamine B. However, no significant increase in percentage removal of Rhodamine B was observed as the dosage of adsorbent increased, probably because of the attainment of equilibrium. This shows that the availability of more adsorbent sites, in terms of adsorbent dosage, would not guarantee the capture of more pollutants under given experimental conditions. Moreover, the percent adsorption of AGW is higher than that of GW due to the removal of limonene and chlorophyll (as was confirmed by the

Table 1 – *Elemental composition of GW and AGW obtained by spot analysis through EDX*

Element	GW (wt%)	AGW (wt%)
C	58.30	62.87
O	37.45	33.57
Si	2.76	3.55
Ca	0.77	0
Fe	0.72	0
Total	100.00	100.00

Table 2 – *Effect of adsorbent dosage and initial pH on the removal percentage of pollutant dye (T = 30 °C, initial concentration = 100 mg L^{-1}, t = 400 min)*

Parameter	Dosage (g)	pH	Removal percentage (%) ± 1	
			GW	AGW
Effect of dose	0.05	6.6±0.1	45.7	54.0
	0.1		52.2	60.2
	0.2		62.3	70.7
	0.5		72.2	88.6
	0.9		79.9	94.2
	1.5		87.2	97.2
	2.2		88.8	98.1
	3		89.9	98.6
	4		90.4	98.7
Effect of pH	0.3	2	51.9	63.7
		3	57.8	64.4
		4	58.6	67.8
		5	61.7	72.7
		6	62.7	76.3
		7	65.5	78.8
		8	69.4	82.7
		9	72.8	83.6
		10	74.1	85.7

Table 3 – *Effect of time on the removal percentage of pollutant dye (T = 30 °C, initial concentration = 100 mg L^{-1}, initial pH = 6.6 ± 0.1, dosage = 0.3 g)*

Time (min)	Removal percentage (%) ± 1	
	GW	AGW
1	38.4	41.5
3	42.5	47.6
5	44.6	51.5
10	46.1	55.2
25	51.2	60.1
50	55.8	64.3
90	59.9	69.4
135	61.5	72.3
180	62.3	74.6
240	63.3	75.7
320	64.0	76.8
390	64.4	77.3

FTIR), which causes a change in physical structure by the formation of irregular cavities on the grass surface after the acidic treatment of grass, and provides more active sites to the Rhodamine B dye, which could be attractive for the adsorption of basic Rhodamine B dye. An amount of 0.3 g of adsorbent was selected for further batch studies.

The solution pH is a key parameter while studying the adsorption potential of an adsorbent. Table 2 shows the influence of pH on the adsorption behavior of GW and AGW. As may be observed from Table 2, the adsorption of Rhodamine B decreased as solution pH decreased, and the maximum adsorption capacity was observed at pH 10. This decrease in uptake capacity was ascribed to the force of repulsion between H^+ ions and the cationic species of the Rhodamine B[41]. The maximum percent removal was observed to be 74.1 and 85.7 for GW and AGW, respectively.

Dynamic analysis

The results of the adsorption of Rhodamine B against time are presented in Table 3. It may clearly be observed that the equilibrium for GW was established earlier than AGW. The GW took around 100 min, while the adsorption onto AGW reached equilibrium after 200 min, as shown in Table 3. A relatively longer time was required for AGW to reach equilibrium, which may be associated with the diffusion of pollutant dye into the cavities present on the surface. Origin (Version 9.1) software was used for the analysis of adsorption dynamics by linear regression of different kinetic models. Table 4 presents a summary of the parametric values of each kinetic model, i.e., pseudo-first and second order intraparticle diffusion, and the Elovich kinetic model. Comparison of the regression coefficient of both models suggested that the regression coefficient (R^2) of the pseudo-first order model was relatively low, i.e., $R^2 \leq 0.95$ for both GW and AGW. However, the adsorption of Rhodamine B on both GW and AGW obeyed the pseudo-second order model as $R^2 = 0.99$ and calculated q_e were much closer to the experimental value. The finest organization of experimental data with a pseudo-second order kinetic model may also be confirmed by the least value of chi-square error, i.e., 0.59 and 0.64 for GW and

Table 4 – *Regression results of kinetic parameters for Rhodamine B adsorption*

Kinetic model	Parameters	GW	AGW
Pseudo-first order	$q_{e,exp}$ (mg g^{-1})	21.4	25.6
	$q_{e,cal}$ (mg g^{-1})	6.49	9.18
	K_1 (1 min^{-1})	0.012	0.013
	R^2	0.95	0.93
	χ^2	1.54	3.63
Pseudo-second order	$q_{e,exp}$ (mg g^{-1})	21.4	25.6
	$q_{e,cal}$ (mg g^{-1})	21.5	25.9
	k_2 (g mg^{-1} min^{-1})	0.010	0.007
	R^2	0.99	0.99
	χ^2	0.59	0.64
Elovich model	α	1.695	1.503
	β	0.64	0.48
	R^2	0.95	0.97
	χ^2	20.24	16.98
Intraparticle diffusion	K_{i1} (mg g^{-1} min$^{-1/2}$)	2.14	2.61
	α_1	13.7	15.5
	R^2	0.99	0.98
	χ^2	1.40	0.097
	K_{i2} (mg g^{-1} min$^{-1/2}$)	1.01	0.19
	α_2	24.4	19.2
	K_{i3} (mg g^{-1} min$^{-1/2}$)	0.08	0.06
	α_3	21.2	20.4
Bangham model	β	–1.77	–1.72
	R^2	0.99	0.99
	χ^2	–0.002	–0.124

AGW, respectively. The agreement of pseudo-second order kinetic model with experimental data reflects that the adsorption of Rhodamine B onto GW and AGW is a concentration-dependent process. Pseudo-second order model cannot highlight the rate-limiting step, which could be either film or pore diffusion within the pores of the solid sorbent. The graphical plot of the intraparticle diffusion model, as shown in Fig. 4, is not linear for the observed time range. It may be seen from Fig. 4 that the plot possesses multi-linear portions, which indicates that more than two steps take part in the adsorption of Rhodamine B. Intraparticle diffusion model rate constant, K_{i1}, has a higher value for AGW than GW, which represents a faster uptake rate at the initial stage. However, the subsequent rate constants, i.e., K_{i2} and K_{i3} become smaller, probably due to diffusion in the cavities on the surface of AGW. The values of α indicate the boundary layer thickness, which is significantly higher in the second phase of the intraparticle diffusion. These higher values in both GW and AGW suggest that surface diffusion plays a major role in the overall adsorption process as a rate-determining step. The dynamic data was further analyzed with Elovich kinetic model. The R^2 value of the Elovich model in Table 4 for both GW and AGW indicated that the surface of adsorbents is heterogamous. However, associated values of chi-square error were higher for GW and AGW in the Elovich model. The regression coefficient (R^2 = 0.99) of the Bangham model for both GW and AGW implied that the boundary layer was not the only rate-limiting step, and that pore diffusion also occurs during the adsorption of Rhodamine B.

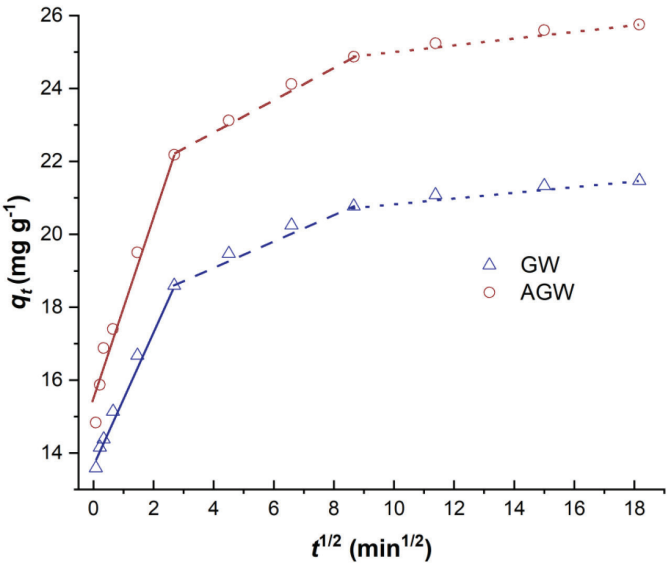

Fig. 4 – *Plot of intraparticle diffusion model*

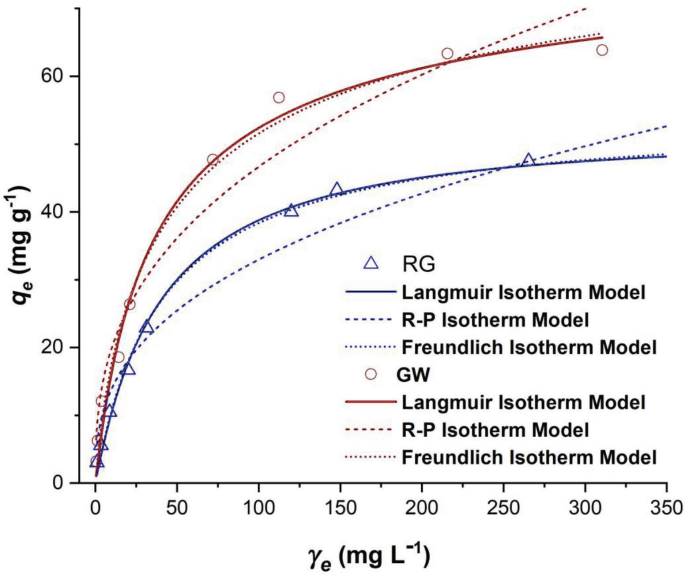

Fig. 5 – *Equilibrium adsorption isotherm modeling for GW and AGW (T = 30 °C, pH = 6.6±0.1, V = 100 mL)*

Isotherm analysis

Fig. 5 shows the equilibrium adsorption isotherm of Rhodamine B onto the investigated GW and AGW. Since the data resembled type I isotherm, three phenomenological isotherm models could be used, namely: Langmuir, Freundlich, and Redlich-Peterson (RP) models. The major difference among these models lies in the way that the heat of adsorption varies with surface coverage. Langmuir supposes constant heat of adsorption because of homogeneous surface, Freundlich assumes a heterogeneous adsorbent surface, and RP isotherm model is the combination of the former two models. The non-linear regression of the experimental adsorption isotherm data for both GW and AGW was performed with Origin 9.1 software, and the results are presented in Fig. 5. The values of the pertinent variables are listed in Table 5.

Freundlich isotherm model exhibited a good fit to the experimental isotherm data at low concentration. However, as the concentration of Rhodamine B increased, the modeled curve tended to deviate from the experimental points, as may be seen in Fig. 5. As a result, poor regression coefficients for GW (R^2 = 0.94) and AGW (R^2 = 0.95) were obtained as listed in Table 3. The value of the regression coefficient (R^2) for the Langmuir model was closer to unity in comparison to the Freundlich isotherm model, and predicted q_e values were better correlated with experimental uptake. Comparison of the goodness of fit of the three-parameter model (i.e., RP isotherm model) with Langmuir showed no improvement in R^2. However, for GW, the q_e of the Langmuir isotherm model showed a relatively smaller value of error function compared to the q_e in the RP isotherm model, and therefore, the adsorption of Rhodamine B on GW may be considered as monolayer adsorption. On the other hand,

Table 5 – *Isotherm model parameters and error analysis for GW and AGW*

Adsorbent/isotherm model	K_L (L g^{-1})	q_{max} (mg g^{-1})		R^2	SABE	χ^2	HYBRID
Langmuir isotherm model							
GW	0.024		54	0.99	2.94	1.77	25.30
AGW	0.027		72.4	0.98	8.81	6.74	96.36
	K_F (L g^{-1})	***N***		R^2	SABE	χ^2	HYBRID
Freundlich isotherm model							
GW	5.9		2.67	0.94	4.29	7.84	111.93
AGW	8.5		2.71	0.95	5.36	8.43	120.44
	K_{RP} (L mg^{-1})	α	β	R^2	SABE	χ^2	HYBRID
R-P isotherm model							
GW	1.27	0.02	1.03	0.99	3.33	1.91	31.76
AGW	2.27	0.04	0.94	0.98	7.51	5.99	99.83

the smallest value of the error function of q_e associated with AGW in the RP isotherm model revealed that the data of the experimental isotherm were well fitted by the three-parameter model rather than the two-parameter models, as summarized in Table 5. Based on the isotherm analysis of AGW, it can be concluded that, at low concentration values, the adsorption of Rhodamine B is monolayer adsorption as the value of the expression $\alpha_R \gamma_e^{\beta}$ is less than 1, and for the higher concentrations, the value of this expression becomes greater than 1, which exhibits the heterogeneous adsorption of Rhodamine B on the adsorbent.

Thermodynamic analysis

The thermodynamic parameters were estimated from the plot of ln(K) vs 1/T (Fig. 6). It is evident from the graphical plot that the adsorption capacity of both GW and AGW increases with the rise in temperature. Table 6 summarizes the values calculated for Gibbs free energy (ΔG), change in entropy (ΔS), and change in enthalpy ($\Delta H°$). The negative number of standard Gibbs energy at all examined temperatures suggested that Rhodamine B adsorption onto both GW and AGW was feasible and spontaneous in nature. The magnitude of Gibbs free energy change was higher for AGW than GW. This could be linked to the removal of chlorophyll and limonene, followed by leaching of metallic impurities that produced more active sites that favored the adsorption of Rhodamine B. The positive value of change in enthalpy showed that the adsorption process was endothermic in nature. Moreover, the enthalpy values were less than 40 kJ mol^{-1} (i.e., 20.3 kJ mol^{-1} and 31.3 kJ mol^{-1} for GW and AGW, respectively), revealing that the process of adsorption of Rhodamine B laid in the physisorption range. The positive value of entropy confirmed the arbitrariness at the solid-liquid interface, reflecting the affinity of the adsorbent surface.

Table 6 – *Thermodynamic parameters for Rhodamine B adsorption onto solid sorbent*

Sample	T(°C)	R^2	ΔG (kJ mol^{-1})	$\Delta H°$ (kJ mol^{-1})	$\Delta S°$ (kJ K^{-1} mol^{-1})
GW	20	0.98	–0.23	20.28	0.07
	30		–0.93		
	40		–1.63		
	50		–2.33		
AGW	20	0.99	–0.95	31.28	0.11
	30		–2.05		
	40		–3.15		
	50		–4.25		

Performance comparison

Table 7 summarized the adsorption capability of various adsorbents, at an optimal dosage and pH level. In this present research, the high comparable capacity for the removal of Rhodamine B was 54 mg g^{-1} and 72.4 mg g^{-1} for grass waste and activated grass waste, respectively. This maximum uptake reflects the maximum surface active site for adsorption in comparison to waste biomass materials, including orange and banana waste powder.

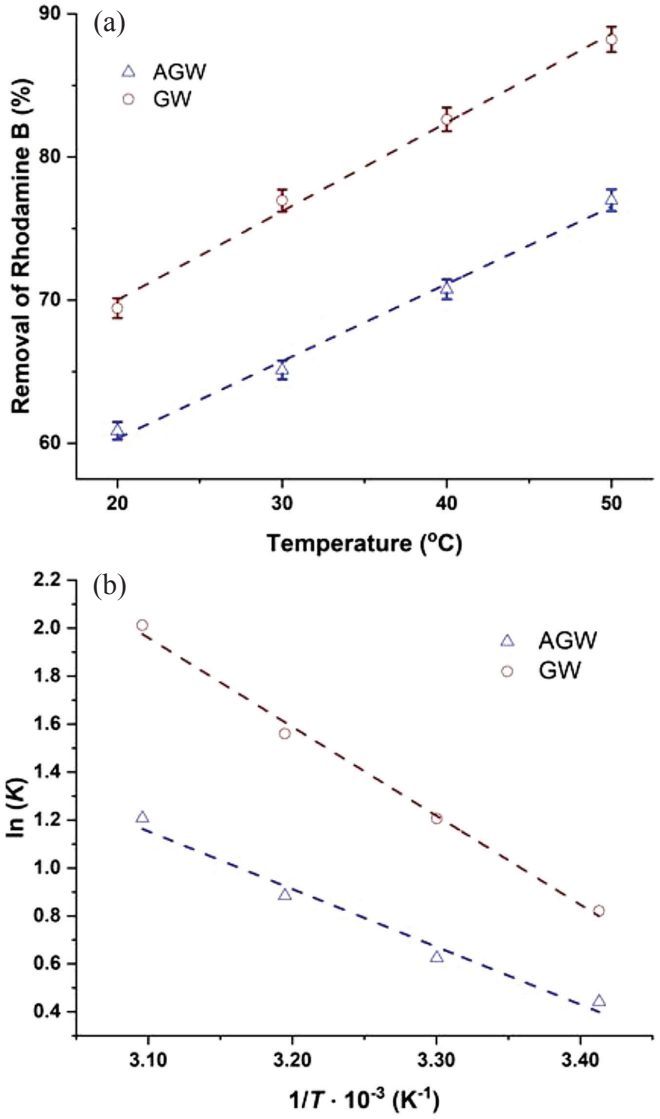

Fig. 6 – *(a) Effect of temperature, and (b) Van't Hoff plot for thermodynamic analysis*

Table 7 – *Comparison of adsorption capacities of various synthesized adsorbents*

Adsorbent	q_e (mg g^{-1})	Reference
Orange peel powder	10.1	(42)
Aleurites moluccana waste seed	119	(43)
Banana peel powder	3.8	(44)
Dika Nuts	53	(45)
Chitosan coated Dika Nuts	217.39	(46)
Calcined mussels shells	45.67	(47)
Carbon nanotubes	3.5	(48)
Casuarina equisetifolia	49.52	(49)
Casuarina equisetifolia	82.34	(50)
Azolla pinnata	72.2	(51)
GW	54	This study
AGW	72.4	This study

Conclusion

Adsorbent based on grass waste was synthesized, and its efficiency in the removal of Rhodamine B from aqueous phase was studied. The process parameters have a substantial effect on the pollutant removal capacity of the adsorbent. The spectroscopic analysis confirms the successful removal of chlorophyll and limonene as a result of alcoholic wash during the activation process. Metallic impurities were also leached out during acid treatment, which is clearly perceptible in the EDX analysis. However, the thermal stability of the activated grass decreased due to the chlorophyll removal, which binds lignin chains in the grass. The adsorption process of Rhodamine B onto GW and AGW is endothermic, and tends to be more spontaneous at a higher temperature. The enthalpy of adsorption was less than 40 kJ mol^{-1} for both GW and AGW, suggesting that the adsorption may be classified as physisorption. Kinetic analysis showed that the adsorption of pollutant dye was diffusion-controlled. The value of the maximum adsorption capacity obtained from the Langmuir isotherm model was 54 mg g^{-1} and 72.4 mg g^{-1} for GW and AGW respectively. Keeping in view the adsorption results, adsorbent synthesized from waste grass could be considered as an alternative to adsorbents for the treatment of colored water.

DATA AVAILABILITY STATEMENT

The authors confirm that the data supporting the findings of this study are available within the article [and/or] its supplementary materials.

ACKNOWLEDGMENTS

Authors acknowledge the Department of Chemical Engineering, University of Engineering and Technology, Lahore, for providing research facilities to conduct this research.

AUTHOR CONTRIBUTIONS

A. A. (Graduate student) conducted all the experiments. A. Z. (Lecturer) wrote the first draft of the manuscript. U. A. (Assistant Professor) revised the material characterization section of the manuscript. Z. A. (Associate Professor) reviewed and revised the whole manuscript. R. A. (Lecturer) revised the experimental results and analysis section of the manuscript. M. M. B. (Research Associate) formatted and edited the manuscript for grammatical mistakes.

FUNDING DETAILS

This research received no specific grant from funding agencies in the public, commercial, or not-for-profit sectors.

CONFLICT OF INTEREST

The authors declare that they have no conflict of interest.

References

1. *Anastopoulos, I., Hosseini-Bandegharaei, A., Fu, J., Mitropoulos, A. C., Kyza*s, *G. Z.*, Use of nanoparticles for dye adsorption: Review, J. Dispers. Sci. Technol. **39** (2018) 836. doi: https://doi.org/10.1080/01932691.2017.1398661
2. *Mehrdad, A., Hashemzadeh*, *R.*, Ultrasonic degradation of rhodamine B in the presence of hydrogen peroxide and some metal oxide, Ultrason. Sonochem. **17** (2010) 168. doi: https://doi.org/10.1016/j.ultsonch.2009.07.003
3. *Liu, K., Li, H., Wang, Y., Gou, X., Duan*, *Y.*, Adsorption and removal of rhodamine B from aqueous solution by tannic acid functionalized graphene, Colloids Surfaces A Physicochem. Eng. Asp. **477** (2015) 35. doi: https:// doi.org/10.1016/j.colsurfa.2015.03.048
4. *Gadekar, M. R., Ahammed, M. M.*, Coagulation/flocculation process for dye removal using water treatment residuals: Modelling through artificial neural networks, Desalin. Water Treat. **57** (2016) 26392. doi: https:// doi.org/ 10.1080/19443994.2016.1165150
5. *Shaban, M., Abukhadra, M. R., Hamd, A., Amin, R. R., Khalek*, *A. A.,* Photocatalytic removal of Congo red dye using MCM-48/Ni_2O_3 composite synthesized based on silica gel extracted from rice husk ash; fabrication and application, J. Environ. Manage. **204** (2017) 189. doi: https://doi.org/10.1016/j.jenvman.2017.08.048
6. *Abid, M. F., Zablouk, M. A., Abid-Alameer*, *A. M.,* Experimental study of dye removal from industrial wastewater by membrane technologies of reverse osmosis and nanofiltration, Iranian J. Environ. Health Sci. Eng. **9** (2012) 17. doi: https://doi.org/10.1186/1735-2746-9-17
7. *Fang, Z., Zhang, K., Liu, J., Fan, J., Zhao*, *Z.,* Fenton-like oxidation of azo dye in aqueous solution using magnetic Fe_3O_4-MnO_2 nanocomposites as catalysts, Water Sci. Eng. **10** (2017) 326. doi: https://doi.org/10.1016/j.wse.2017.10.005
8. *Gupta, V. K., Suhas*, Application of low-cost adsorbents for dye removal – a review, J. Environ. Manage. **90** (2009) 2313. doi: https://doi.org/10.1016/j.jenvman.2008.11.017
9. *Hameed, B. H.*, Grass waste: a novel sorbent for the removal of basic dye from aqueous solution, J. Hazard. Mater. **166** (2009) 233. doi: https://doi.org/10.1016/j.jhazmat.2008.11.019
10. *Toumi, L. B., Hamdi, L., Salem, Z., Allia*, *K.,* Batch adsorption of methylene blue from aqueous solutions by untreated alfa grass, Desalin. Water Treat. **53** (2015) 806. doi: https://doi.org/10.1080/19443994.2013.846236
11. *Ramaraju, B., Reddy, P. M. K., Subrahmanyam, C.*, Low cost adsorbents from agricultural waste for removal of dyes, Environ. Prog. Sustain. Energy. **33** (2014) 38. doi: https://doi.org/10.1002/ep.11742
12. *Alshabanat, M., Alsenani, G., Almufarij, R.*, Removal of crystal violet dye from aqueous solutions onto date palm fiber by adsorption technique, J. Chem. **2013** (2013) 1. doi: https://doi.org/10.1155/2013/210239
13. *Karim, S. K. A., Lim, S. F., Chua, S. N. D., Salleh, S. F., Law, P. L.*, Banana fibers as sorbent for removal of acid green dye from water, J. Chem. **2016 (**2016) 1. doi: https://doi.org/10.1155/2016/9648312
14. *Qiu, Y., Zheng, Z., Zhou, Z., Sheng, G. D.*, Effectiveness and mechanisms of dye adsorption on a straw-based biochar, Bioresour. Technol. **100** (2009) 5348. doi: https://doi.org/10.1016/j.biortech.2009.05.054
15. *Tahir, H., Sultan, M., Akhtar, N., Hameed, U., Abid*, *T.,* Application of natural and modified sugar cane bagasse for the removal of dye from aqueous solution, J. Saudi Chem. Soc. **20** (2016) S115. doi: https://doi.org/10.1016/j.jscs.2012.09.007
16. *Kooh, M. R. R., Dahri, M. K., Lim, L. B. L.*, Removal of the methyl violet 2B dye from aqueous solution using sustainable adsorbent *Artocarpus odoratissimus* stem axis, Appl. Water Sci. **7** (2017) 3573. doi: https://doi.org/10.1007/s13201-016-0496-y
17. *Lim, L. B. L., Priyantha, N., Chan, C. M., Matassan, D., Chieng, H. I., Kooh, M. R. R.*, Investigation of the sorption characteristics of water lettuce (WL) as a potential low-cost biosorbent for the removal of methyl violet 2B, Desalin. Water Treat. **57** (2016) 8319. doi: https://doi.org/10.1080/19443994.2015.1017740
18. *Lim, L. B. L., Priyantha, N., Mansor, N. H. M.*, *Artocarpus altilis* (breadfruit) skin as a potential low-cost biosorbent for the removal of crystal violet dye: Equilibrium, thermodynamics and kinetics studies, Environ. Earth Sci. **73** (2015) 3239. doi: https://doi.org/10.1007/s12665-014-3616-8
19. *Ahmad, M. A., Ahmad, N., Bello, O. S.*, Modified durian seed as adsorbent for the removal of methyl red dye from aqueous solutions, Appl. Water Sci. **5** (2015) 407. doi: https://doi.org/10.1007/s13201-014-0208-4
20. *Mafra, M. R., Igarashi-Mafra, L., Zuim, D. R., Vasques, É. C., Ferreira, M. A.*, Adsorption of remazol brilliant blue on an orange peel adsorbent, Brazilian J. Chem. Eng. **30** (2013) 657. doi: https://doi.org/10.11113/jt.v74.4882
21. *Yao, S., Lai, H., Shi, Z.*, Biosorption of methyl blue onto tartaric acid modified wheat bran from aqueous solution, Iranian J. Environ. Health Sci. Eng. **9** (2012) 16. doi: https://doi.org/10.1186/1735-2746-9-16
22. *Kumar, K. V., Porkodi, K.*, Mass transfer, kinetics and equilibrium studies for the biosorption of methylene blue using Paspalum notatum, J. Hazard. Mater. **146** (2007) 214. doi: https://doi.org/10.1016/j.jhazmat.2006.12.010
23. *Chen, L., Lü, L., Shao, W., Luo, F.*, Kinetics and equilibria of Cd(II) adsorption onto a chemically modified lawny grass with H[BTMPP], J. Chem. Eng. Data **56** (2011) 1059. doi: https://doi.org/10.1021/je101037x
24. *Sharma, N., Tiwari, D. P., Singh, S. K.*, Decolourisation of synthetic dyes by agricultural waste-a review, Int. J. Sci. Eng. Res. **3** (2012) 385. doi: https://doi.org/10.1515/9783110292855.1
25. *Kumar, M., Pal, A., Singh, J., Garg, S., Bala, M., Vyas, A., Khasa, Y. P., Pachouri, U. C.,* Removal of chromium from water effluent by adsorption onto *Vetiveria zizanioides* Anabaena species, Nat. Sci. **5** (2013) 341. doi: https://doi.org/10.4236/ns.2013.53047

26. *Cheung, C. W., Porter, J. F., McKay, G.*, Elovich equation and modified second-order equation for sorption of cadmium ions onto bone char, J. Chem. Technol. Biotechnol. **75** (2000) 963. doi: https://doi.org/10.1002/1097-4660(200011)75:11<963::AID-JCTB302>3.0.CO;2-Z
27. *Selçuk, N. Ç., Kubilay, Ş., Savran, A., Kul*, *A. R.,* Kinetics and thermodynamic studies of adsorption of methylene blue from aqueous solutions onto paliurus spina-christi mill. frutis and seeds, IOSR J. Appl. Chem. **10** (2017) 53. doi: https://doi.org/10.9790/5736-1005015363
28. *Kumar, A., Jha, A.*, Anticandidal Agents, Academic Press, USA, 2017, 63–71.
29. *Zahir, A., Aslam, Z., Kamal, M. S., Ahmad, W., Abbas, A., Shawabkeh, R. A.*, Development of novel cross-linked chitosan for the removal of anionic Congo red dye, J. Mol. Liq. **244** (2017) 211. doi: https://doi.org/10.1016/j.molliq.2017.09.006
30. *Enayatpour, B., Rajabi, M., Moradi, O., Asdolehzade, N., Nayak, A., Agarwal, S., Gupta, V. K.,* Adsorption kinetics of lysozyme on multi-walled carbon nanotubes and amino functionalized multi-walled carbon nanotubes from aqueous solution, J. Mol. Liq. **254** (2018) 93. doi: https://doi.org/10.1016/j.molliq.2018.01.079
31. *Belhachemi, M., Addoun, F.*, Comparative adsorption isotherms and modeling of methylene blue onto activated carbons, Appl. Water Sci. **1** (2011) 111. doi: https://doi.org/10.1007/s13201-011-0014-1
32. *Ho, Y., Chiu, W., Wang, C.*, Regression analysis for the sorption isotherms of basic dyes on sugarcane dust, Bioresour. Technol. **96** (2005) 1285. doi: https://doi.org/10.1016/j.biortech.2004.10.021
33. *Amrhar, O., Nassali, H., Elyoubi, M. S.*, Application of nonlinear regression analysis to select the optimum absorption isotherm for methylene blue adsorption onto natural illitic clay, Bull. la Société R. des Sci. Liège, **84** (2015) 116. doi: https://popups.uliege.be:443/0037-9565/index.php?id=4865
34. *Komnitsas, K., Zaharaki, D., Bartzas, G., Kaliakatsou, G., Kritikaki, A.*, Efficiency of pecan shells and sawdust biochar on Pb and Cu adsorption, Desalin. Water Treat. **57** (2014) 3237. doi: https://doi.org/10.1080/19443994.2014.981227
35. *Aslam, U., Ramzan, N., Iqbal, T., Kazmi, M., Ikhlaq, A.*, Effect of demineralization on the physiochemical structure and thermal degradation of acid treated indigenous rice husk, Polish J. Chem. Technol. **18** (2016) 117. doi: https://doi.org/10.1515/pjct-2016-0057
36. *Mohaptra, S., Dash, P. K., Behera, S. S., Thatoi, H.*, Optimization of delignification of two Pennisetum grass species by NaOH pretreatment using Taguchi and ANN statistical approach, Environ. Technol. **37** (2016) 940. doi: https://doi.org/10.1080/09593330.2015.1093034
37. *Boon, T. H., Raheem, A., Ghani, W. A., Hussain, S. A., Sum, D. N. K.*, Thermogravimetric study of napier grass in inert and oxidative atmospheres conditions, J. Phy. Sci. **28** (2017) 155. doi: https://doi.org/10.21315/jps2017.28.s1.10
38. *Aslam, U., Ramzan, N., Aslam, Z., Iqbal, T., Sharif, S., Hasan, S. W., Malik, A.*, Enhancement of fuel characteristics of rice husk via torrefaction process, Waste Manag. Res. **37** (2019) 737. doi: https://doi.org/10.1177/0734242X19838620
39. *Jia, L., Yao, X., Ma, J., Long, C.*, Adsorption kinetics of water vapor on hypercrosslinked polymeric adsorbent and its comparison with carbonaceous adsorbents, Microporous Mesoporous Mater. **241** (2017) 178. doi: https://doi.org/10.1016/j.micromeso.2016.12.028
40. *Karimi, K., Taherzadeh, M. J.*, A critical review on analysis in pretreatment of lignocelluloses: Degree of polymerization, adsorption/desorption, and accessibility, Bioresour. Technol. **203** (2016) 348. doi: https://doi.org/10.1016/j.biortech.2015.12.035
41. *Oyekanmi, A. A., Ahmad, A., Hossain, K., Rafatullah, M.*, Adsorption of Rhodamine B dye from aqueous solution onto acid treated banana peel: Response surface methodology, kinetics and isotherm studies, PLoS One **14** (2019) 1. doi: https://doi.org/10.1371/journal.pone.0216878
42. *Daouda, A., Honorine, A. T., Bertrand, N. G., Richard, D.*, Adsorption of Rhodamine B onto Orange Peel Powder, American J. Chem. **9** (2019) 142. doi: https://doi.org/10.5923/j.chemistry.20190905.02
43. *Postai, D. L., Demarchi, C. A., Zanatta, F., Melo, D. C. C., Rodrigues, C. A.*, Adsorption of rhodamine B and methylene blue dyes using waste of seeds of *Aleurites Moluccana*, a low cost adsorbent, Alexandria Eng. J. **55** (2016) 1713. doi: https://doi.org/10.1016/j.aej.2016.03.017
44. *Singh, S., Parveen, N., Gupta, H.*, Adsorptive decontamination of rhodamine-B from water using banana peel powder: A biosorbent, Environ. Technol. Innov. **12** (2018) 189. doi: https://doi.org/10.1016/j.eti.2018.09.001
45. *Inyinbor, A. A., Adekola, F. A., Olatunji, G. A.*, Adsorption of Rhodamine B dye from aqueous solution on *Irvingia gabonensis* biomass: Kinetics and thermodynamics studies, South African J. Chem. **68** (2015) 115. doi: https://doi.org/10.17159/0379-4350/2015/v68a17
46. *Inyinbor, A. A., Adekola, F. A., Olatunji, G. A.*, Liquid phase adsorptions of Rhodamine B dye onto raw and chitosan supported mesoporous adsorbents: Isotherms and kinetics studies, Appl. Water Sci. **7** (2017) 2297. doi: https://doi.org/10.1007/s13201-016-0405-4
47. *Haddad, M. E., Regti, A., Laamari, M. R., Slimani, R., Mamouni, R., Antri, S. E., Lazar, S.*, Calcined mussel shells as a new and eco-friendly biosorbent to remove textile dyes from aqueous solutions, J. Taiwan Inst. Chem. Eng. **45** (2014) 533. doi: https://doi.org/10.1016/j.jtice.2013.05.002
48. *Kumar, S., Bhanjana, G., Jangra, K., Dilbaghi, N., Umar, A.*, Utilization of carbon nanotubes for the removal of rhodamine B dye from aqueous solutions, J. Nanosci. Nanotechnol. **14** (2014) 4331 doi: https://doi.org/10.1166/jnn.2014.8077
49. *Dahri, M. K., Kooh, M. R. R., Lim, L. B. L.*, Remediation of Rhodamine B dye from aqueous solution using *Casuarina equisetifolia* cone powder as a low-cost adsorbent, Adv. Phy. Chem. **2016** (2016) 1. doi: https://doi.org/10.1155/2016/9497378
50. *Kooh, M. R. R., Dahri, M. K., Lim, L. B. L.*, The removal of rhodamine B dye from aqueous solution using *Casuarina equisetifolia* needles as adsorbent, Cogent Environ. Sci. **2** (2016) 1140553. doi: https://doi.org/10.1080/23311843.2016.1140553
51. *Kooh, M. R. R., Lim, L. B. L., Lim, L. H., Dahri, M. K.*, Separation of toxic rhodamine B from aqueous solution using an efficient low-cost material, *Azolla pinnata*, by adsorption method, Environ. Monit. Assess. **188** (2016) 108. doi: https://doi.org/10.1007/s10661-016-5108-7